ARCHIVE OF MECHANICAL ENGINEERING

DOI: 10.24425/ame.2026.158901 Early Access; pp. 1–23

Muhammad WAQAS[1], Aneeq RAHEEM[2], Waseem SIDDIQUE[2], Khalid WAHEED[1], Muhammad ZAKI[3]

Investigation of heat transfer enhancement in impinging jet-dimpled-protruded solar air heaters

Received 09 November 2025, **Revised** 03 February 2026, **Accepted** 15 February 2026, **Published online** 06 May 2026

Keywords: Solar Air Heaters (SAH), dimple/protrusion surfaces, jet impingement, computational fluid dynamics, heat transfer enhancement, Nusselt number

Solar energy is a source of renewable energy and is considered a clean, convenient, sustainable, safe, abundant, and economical source. Solar Air Heaters (SAHs) are one of the applications of solar energy. SAH has a wide variety of applications but has low thermal efficiency. This low thermal efficiency is due to the low thermal capacity of the air, and the poor process of heat transfer between the absorbing plate channel and air. With the aim to improve thermal efficiencies, the novel dimple/protrusion surfaces have been incorporated onto the 307×212 mm aluminum absorbing plate. A 3×3 array of 5 mm impinging jets is used to further decrease the temperature of the plate. A set of five different plate configurations, i.e., smooth, dimpled, dimpled-protruded, protruded-dimpled, and protruded configurations are simulated by using the experimentally validated Computational Fluid Dynamics (CFD) model. The values of heat transfer enhancement, pressure drop, and Thermal Performance Factor were evaluated from the CFD study. The protruded plate is selected as the best plate configuration, based on the Thermal Performance Factor. An overall improvement of 33.5% is observed in the current research work, as compared to the smooth configuration. Hence promising is the augmentation.

✉ Aneeq RAHEEM, e-mail: aneeqraheem1@gmail.com

[1]Department of Nuclear Engineering, Pakistan Institute of Engineering and Applied Sciences, Pakistan, 456501

[2]Department of Mechanical Engineering, Pakistan Institute of Engineering and Applied Sciences, Pakistan, 456501

[3]Department of Chemical Engineering, Pakistan Institute of Engineering and Applied Sciences, Pakistan, 456501

Nomenclature

Abbreviations

A	area, m^2
D_h	hydraulic diameter, m
D_i	imprint diameter, m
h	coefficient of convective heat transfer, W/m^2K
,k	thermal conductivity, W/mK
q	net heating power, W
q''	heat flux, W/m^2
Q	volume flow rate, m^3/s
R	resistance of heating coils, Ω
T	temperature, °C
v	velocity of air, m/s
V	voltage applied across heater, V
ΔP	pressure drop, Pa
ΔT	temperature difference, °C or K

Greek Symbols

Δ	difference, –
η	thermal performance factor, –
υ	kinematic viscosity, m^2/s
ρ	density, kg/m^3

Dimensionless terms

f	coefficient of friction (friction factor)
f/f_o	friction factor ratio
H/D_i	height/imprint diameter
Nu	Nusselt number
Nu/Nu_o	heat transfer enhancement
P/D_i	pitch/imprint diameter
Re	Reynolds number

1. Introduction

Global energy demand is going to increase by 35% in the next two decades [1]. This is mainly due to the projected growth in world population, and the economic and industrial growth of developing countries. While the energy demand is increasing, the increase in energy resources is not linear. Therefore, researchers are putting their efforts into the field of improving the efficiency of existing products. These products include heat exchangers, coolers, chillers, Solar Air Heaters (SAHs), and much more. The ultimate benefit of the research is the improved heat transfer in a variety of practical applications such as electronic components, heat exchangers, micro-fluidic passages, turbine blades, and even biomedical devices in continuous

operation. The use of artificial roughness on a surface is an effective technique to enhance heat transfer to fluid flowing in ducts [2].

Solar energy is converted directly into electrical power by photovoltaic modules, while solar collectors convert solar energy into thermal energy. Solar collector works by absorbing direct solar radiation and converting it into thermal energy, which can be stored in the form of sensible heat, latent heat, or a combination of sensible and latent heat. Heat transfer enhancement in the SAHs can be achieved by breaking the laminar sub-layer near the absorbing surface. The enhancement in heat transfer is at the expense of an increase in pressure drop. The adverse thermodynamic properties of the air, such as its low density and low heat capacity, have led to poor heat transfer from the absorber plate of SAHs. This have ultimately reduced the efficiency of SAHs. Consequently, several techniques such as roughness elements, i.e., ribs [3–6] corrugation [7–9] dimples [10], and inserts [11], have been developed to improve the thermal performance of SAHs. Alternatively, several researchers used nanofluids [12], and molten salts [13], as the working medium to increase the heat transfer.

A number of studies are extensively available in the literature to enhance the efficiency of SAHs. Geometric and flow parameters are the key factors in increasing heat transfer. Previous studies have shown that dimples/protrusions configurations can provide a substantial improvement in heat transfer with a relatively low-pressure loss compared to the other types of augmented heat transfer devices. Vortex formation at the surface of the dimple/protrusion is responsible for the mixing of the fluid streams. Cold air outside the thermal boundary layer gets in contact with the wall and is heated. Many researchers presented a comparative study of various configurations of dimples. Saini et al. [14] investigated the effect of roughness height and operating parameters like the Reynolds number on heat transfer and friction factor with dimple-shape roughness geometry. According to these investigators, heat transfer can be enhanced considerably as a result of providing dimple-shape roughness geometry on the absorber plate of a SAH duct. The maximum value of the Nusselt number has been found to correspond to a relative roughness height (e/D) of 0.0379 and a relative pitch (p/e) of 10. In recent years, heat transfer enhancement in SAHs using roughness geometry has gained much attention. Goel et al. [15] experimented with the effect of roughness and flow parameters on the heat collector plate of SAHs using hemispherical dimple cavities. Results show that the higher heat transfer is at the trailing edge in comparison to the leading edge of the dimple.

Performance analysis of SAHs is complicated because of the absence of statistical correlation for heat transfer and friction factor. Kumar [2] developed the statistical correlations for the Nusselt number and friction factor in terms of roughness and flow parameters. These were derived for the dimple roughened ducts based on the experimental data. It was concluded that an increase in depth to depth-to-diameter ratio resulted in an increase in the Nusselt number. Hassan et al. [16] experimentally investigated the effect of roughness on the Nusselt num-

ber and friction factor on novel multiple arc dimple-roughened SAHs. An increase of 3.19–5.56 times was revealed in the Nusselt number as compared to the smooth case. Perwez et al. [17] tested the spherical dimple plate SAHs and reported an increase of 23.45% to 35.5% in thermal efficiency as compared to flat plate SAHs.

In most industrial applications, jets are considered an efficient means of transferring energy and mass. These include the cooling of turbine blades [18], solar applications [19], electronic components [20], critical machine parts and the cooling of materials during molding processes. The impact of the jet causes a sudden expansion of the fluid stream that in turn causes high heat transfer rates. Impinging jets break the typical streamwise flow that exists in the conventional flat plate collector and create a flow boundary layer between the solid absorber plate and air interface. Nadda et al. [21] experimentally studied the influence of jet impingement with multi-protrusion obstacles and developed the correlations for the Nusselt number and friction factor with a difference of ±9% and ±11% from experimental results. Rajaseenivasan et al. [22] examined the effect of the angle of attack of the impact jets on the performance of the SAHs. Results reveal that the highest performance is achieved with a 30° angle of attack. An optimized performance is observed with the 5 mm diameter hole as the decrease in jet diameter causes increases in pressure loss. With a flow rate of 0.016 kg/s, the maximum thermal enhancement factor of 2.19 and an efficiency of 55.8% is determined. Chauhan et al. [23] conducted an experimental study to examine the effect of flow and geometrical parameters of jet impingement and the results show a considerable enhancement in heat transfer by a factor of 2.67. Aboghrara et al. [24] investigated the outlet temperature and efficiency of the SAHs. The investigation concluded that the mass flow rate of air greatly influences the heat transfer on SAHs. The proposed design duct is observed to exhibit a 14% increase in thermal efficiency as compared to the smooth duct. Mithani et al. [25] analyzed the inclined impinging jets on the absorber plate of the SAHs. The increase in the Nusselt number and friction factor is about 3.25 and 8.45 times, respectively. Singh et al. [26] conducted an experimental and numerical study using the circular jets on a double pass SAHs and the results showed the improved thermal performance of SAHs with jet impingement as compared to the conventional SAHs.

Numerical simulations are an effective means of investigating the details of flow fields and heat transfer characteristics, resulting from jet impingement and other geometric parameters. Matheswaran et al. [27] studied the single pass, and double duct of SAHs with jet impingement for different mass flow rates, streamwise and spanwise pitch ratios, and jet diameter ratios. The overall performance was assessed by taking into account the energy gain as well as the work input in the form of pumping power. The results show an efficiency increase of 21.2% and exergy efficiency of 22.4% as compared to the single pass, single duct of jet plate SAHs. Yadav et al. [28] simulated the 3D fluid domain of SAHs using the k-ε turbulence model. With a jet height ratio of 0.216, a jet diameter ratio of 0.065,

and the Reynolds number of 15 500, the maximum thermal-hydraulic factor of 3.66 was obtained. Alam et al. [29] numerically studied the protrusion rib roughness on the absorber plate of the SAHs. The parallel flow configuration shows an overall efficiency of 69.88%.

From the above literature review, it can be concluded that a lot of studies are available in the literature, which concern heat transfer enhancement in SAHs. Most of the researchers explored the performance of dimple/protrusion and jet impingement individually. The combined effect of both cooling techniques needs to be explored in detail. To the best of the author's knowledge, no study is available on the perpendicular configuration with multiple jet impingement on different plate configurations like spherical dimples/protrusions and their combinations, over a wide range of Reynolds numbers and other geometrical parameters.

Therefore, the objectives of the present study are:

- To select the optimized plate configuration by simulating the five different dimple/ protrusion plate configurations using the validated CFD model.
- To select the best case having maximum heat transfer with minimal pressure losses, i.e., higher thermal performance factor.

2. Methodology

An appropriate design methodology for SAH heating channels is needed for efficient heat transfer. A combination of jet impingement with an artificial roughened surface was used to increase the overall heat transfer from the absorber plate of the SAHs. The experimentation was performed on a dimpled plate with an imprint diameter (D) of 20 mm, Height/Imprint Diameter ratio (H/D) of 0.1, and Pitch/Imprint Diameter ratio (P/D) of 0.8 at the Reynolds number of 3000. CFD results were validated with the experimental results. Using the validated CFD model, five plate configurations, including the smooth plate, were simulated, and the optimized one was selected. The CFD tool was selected as the viable tool for the current research, as it reduces the experimental cost, time, and safety hazards. Moreover, it also shows the complete 3-D flow and thermal profiles. Fig. 1 shows the overall research methodology for heat transfer enhancement in SAHs.

3. Experimental details

3.1. Experimental setup

Based on all the information obtained from the literature review and the design of the experiment, a test rig was designed to measure heat transfer and pressure drop on dimple/protrusion channels with jet impingement. Fig. 2 shows the simplified diagram of the apparatus being used for heat transfer. The flow system consisted of an air blower, a flow meter, an entrance region, a test section, and an exit section.

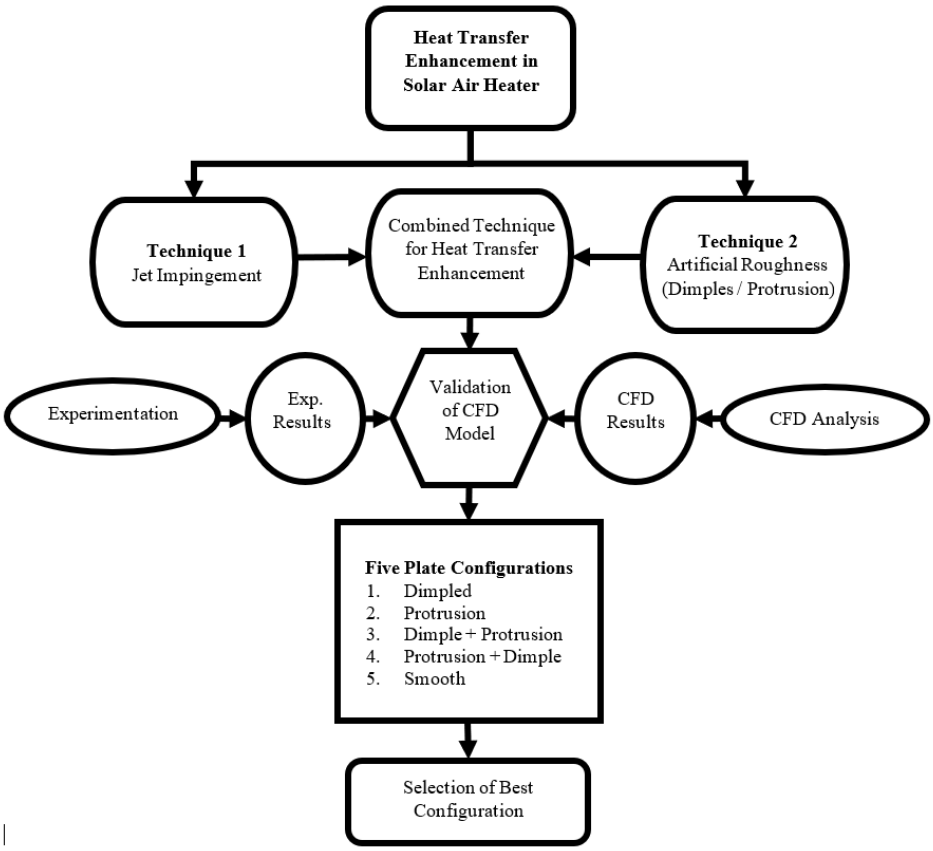

Fig. 1. Research methodology for heat transfer enhancement in SAHs

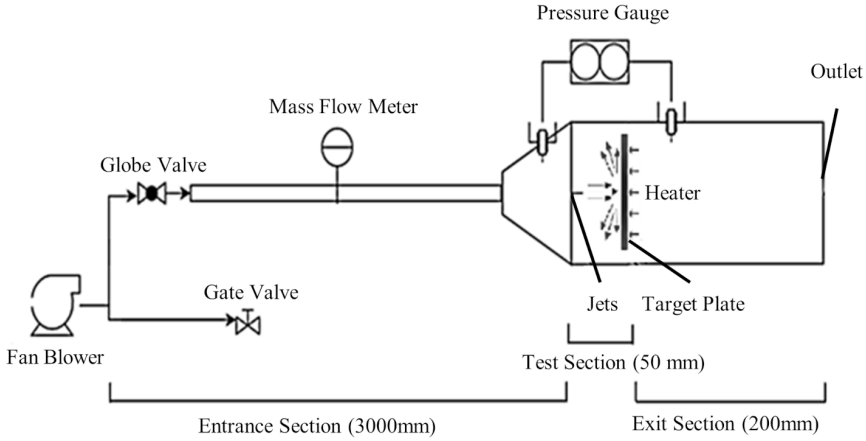

Fig. 2. Schematic diagram of experimental setup

The working fluid was the ambient air, which was supplied with the help of a 550-watt centrifugal air blower. A globe valve and a gate valve were installed after the blower downstream to regulate the flow rate of air. The length of the entrance region and exit section was provided as 3000 mm and 100 mm, respectively. A conical diffuser-type duct section was formed so that pressure could be increased. The duct, after the diffuser section, having the dimensions of 463 mm × 401 mm with an aspect ratio of 1.16 was made of galvanized iron sheets. The acrylic jet plate was flanged in the test section such that the middle jet hit the center of the target plate. The distance between the jets and the target plate was 45 mm. A 3 × 3 array of square-shaped jets was milled in the middle of the jet plate. The hydraulic diameter of jets and the inter jets spacings were 5.02 mm. Air at very high velocity was exited from the jet plate after which it entered the rectangular test section. A 5-mm-thick aluminum sheet with having roughened surface on its front side was provided as an absorber plate inside the test section. The heated plate was attached to a variable power electric heater having a size of 307 mm by 212 mm with a maximum power of 2400 watts.

A 50 mm thick layer of glass wool as an insulating material was provided in order to minimize the heat losses from the backside of the heater assembly. After the impingement, the air was exited from the test section at a very low velocity. The pressure drop across the test section was measured with the help of pressure transducers. The mass flow rate of air was measured by means of a calibrated orifice meter connected upstream of the test section. Calibrated K-type thermocouples were used to measure the temperature of incoming air and absorbing plate temperature at different locations as shown in Fig. 3. A Data Acquisition Card was used to indicate the output of the thermocouples on the computer. The details of an experimental setup can be found in the previous studies of Raheem et al. [30].

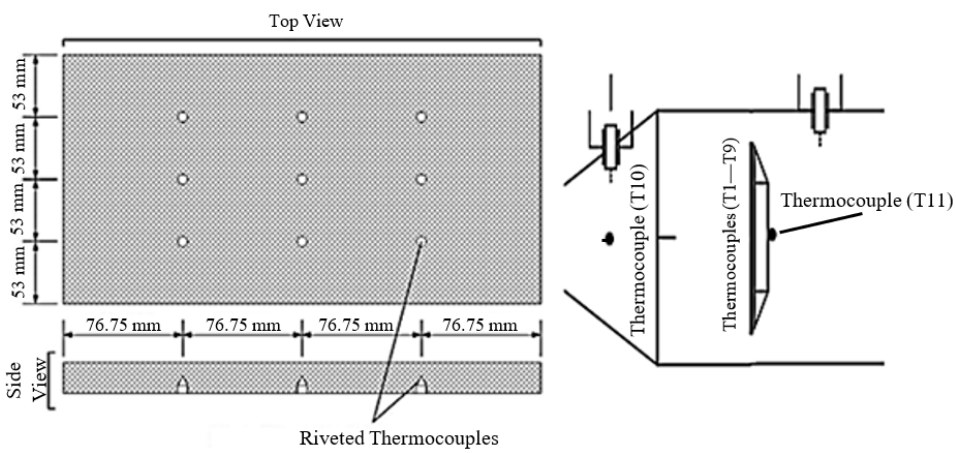

Fig. 3. Placement of thermocouples on target plate

3.2. Roughness geometry

Fig. 4 shows a total of five plate configurations, which were studied to select the optimized plate configuration. Fig. 5 shows different plate configurations with a D_i of 20 mm, pitch of 25 mm, and H/D_i ratio of 0.1. All of the plate configurations have the same geometrical parameters. The difference between the last two cases is the relative position of the plate with respect to the impinging jets. Fig. 5 shows the dimensions of the roughness geometry of the dimple shape, which has been investigated under the present investigation.

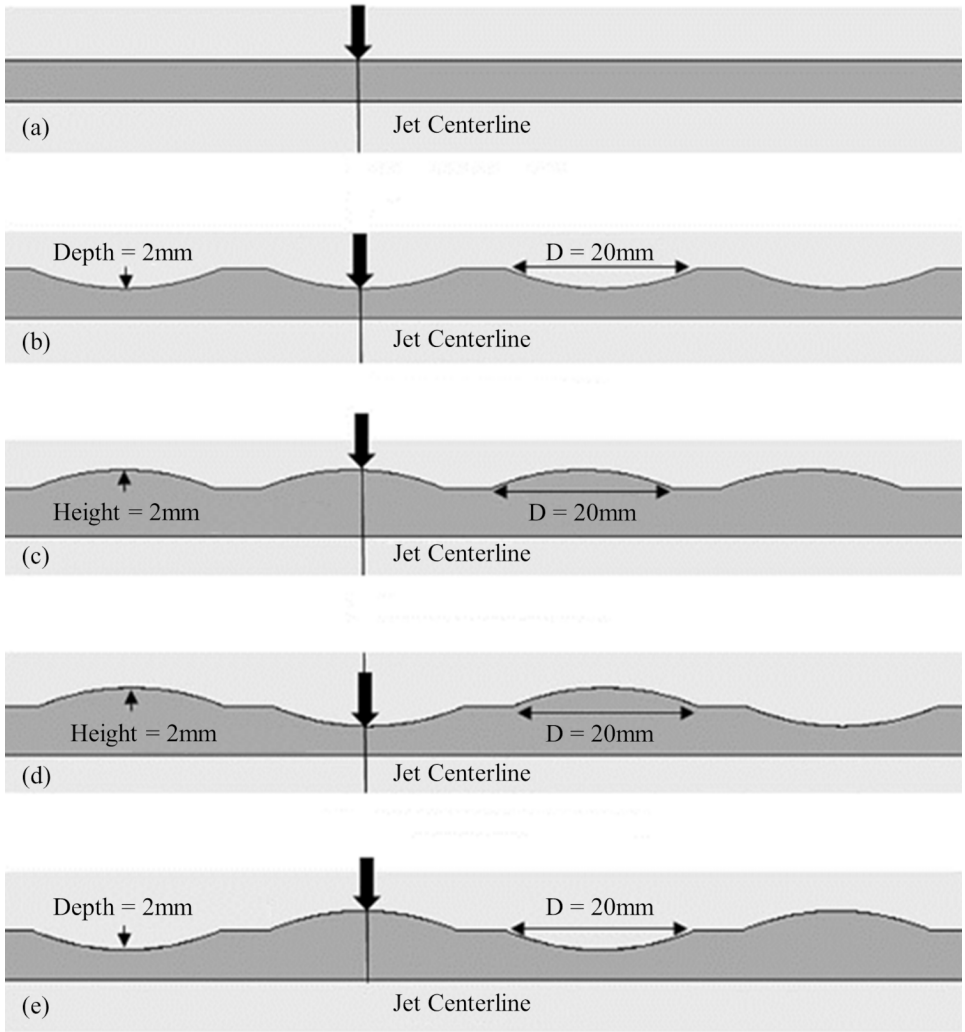

Fig. 4. (a) Smooth plate; (b) Dimple plate; (c) Protrusion plate; (d) Dimple-Protrusion plate; (e) Protrusion-Dimple plate

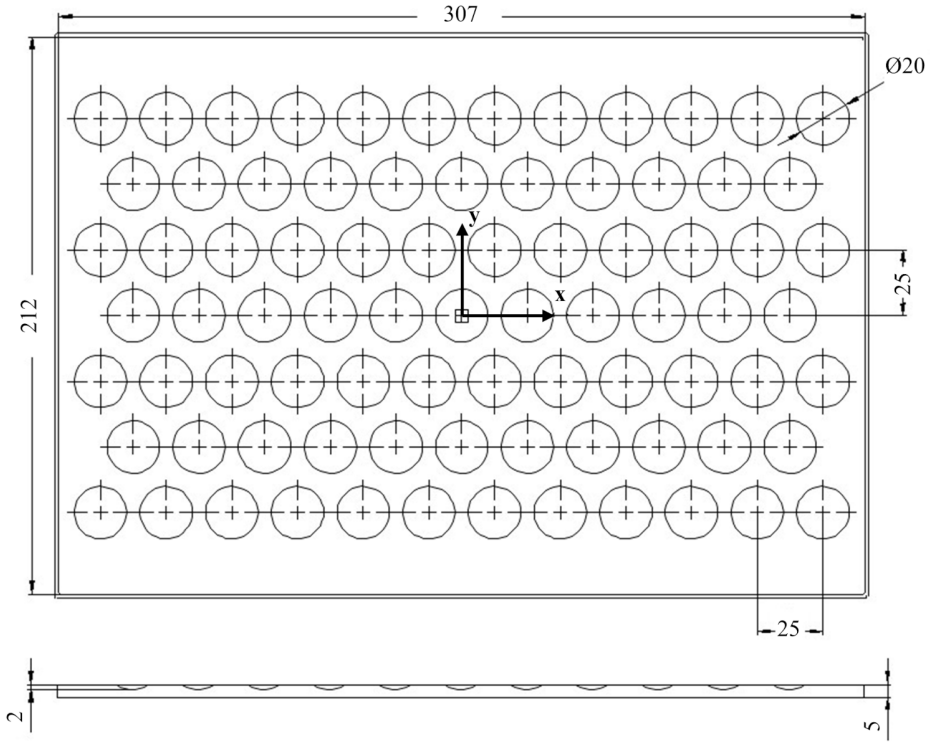

Fig. 5. The dimensions of roughness geometry (All the dimensions are in millimeters (mm))

3.3. Experimental procedure

The test was conducted to collect the relevant data of heat transfer and flow friction under steady-state conditions. The required flow rate of 0.0013 kg/s (corresponding to the Reynolds number of 3360) and heat flux of 330 W/m^2 was achieved by adjusting the globe valve and transformer voltage respectively. The system was allowed to attain a steady state before the data were recorded. The following parameters were measured.

- Temperature of nine k-type thermocouples on the absorber plate surface and at the inlet of the test section.
- Temperature at the outer surface of insulation for conduction losses.
- Pressure drop values across the test section.

3.4. Data reduction

Steady-state temperature values of the target plate at various locations were used to determine the overall average plate temperature ($\overline{T_p}$). The incoming air temperature (T_{bulk}) was measured using thermocouple T_{10}. The heat transfer coef-

ficient, h, was calculated by using the following Eq. (1):

$$\overline{h} = \frac{q''_{\text{actual}}}{\overline{T_p} - T_{\text{bulk}}}, \tag{1}$$

where

$$q''_{\text{actual}} = q'' - q''_{\text{condution losses}}. \tag{2}$$

The average Nusselt number was then calculated using the following Eq. (3):

$$\overline{\text{Nu}} = \frac{\overline{h}\, D_h}{k}, \tag{3}$$

where D_h is the hydraulic diameter of jets and k is the thermal conductivity of air. The friction factor was determined from the measured values of pressure drop ΔP across the test section length using the following Eq. (4).

$$f = \frac{2\Delta P D_h}{L\rho v^2}, \tag{4}$$

where L is the length of the target plate and v is the mean velocity of the air leaving the jets. The thermal performance factor was used to examine the optimized plate configuration. CFD simulations were conducted for smooth ducts under similar conditions. The results of the Nusselt number and friction factor determined for the smooth configurations were used to normalize the results obtained from other plate configurations. The thermal performance factor was calculated using the following Eq. (5). It is the ratio of the improvement in heat transfer at the expense of the increase in friction factor (pressure loss penalty).

$$\eta = \frac{\left(\dfrac{\text{Nu}}{\text{Nu}_o}\right)}{\left(\dfrac{f}{f_o}\right)^{1/3}}. \tag{5}$$

3.5. Uncertainty analysis

Due to uncertainty in measurement in different measuring devices, the error propagates further in calculations. The propagation of error in heat transfer coefficient, the Nusselt number, friction factor, and the thermal performance factor of dimpled plate configuration was calculated based on the basic rules of propagation. The maximum possible measurement errors in the values of the major parameters of the present investigation are given below: The further details of uncertainty analysis can be referred to from the previous study of Raheem et al. [30].

- Uncertainty in temperature difference = 5.3%
- Uncertainty in heat transfer coefficient = 5.9%
- Uncertainty in the Nusselt number = 5.97%
- Uncertainty in friction factor = 5.4%
- Uncertainty in thermal performance factor = 6.1%.

4. Computational details

Fig. 6 shows the schematic diagram of the CFD fluid domain. Air flows in the negative Z direction and strikes the absorber plate facing the positive Z direction.

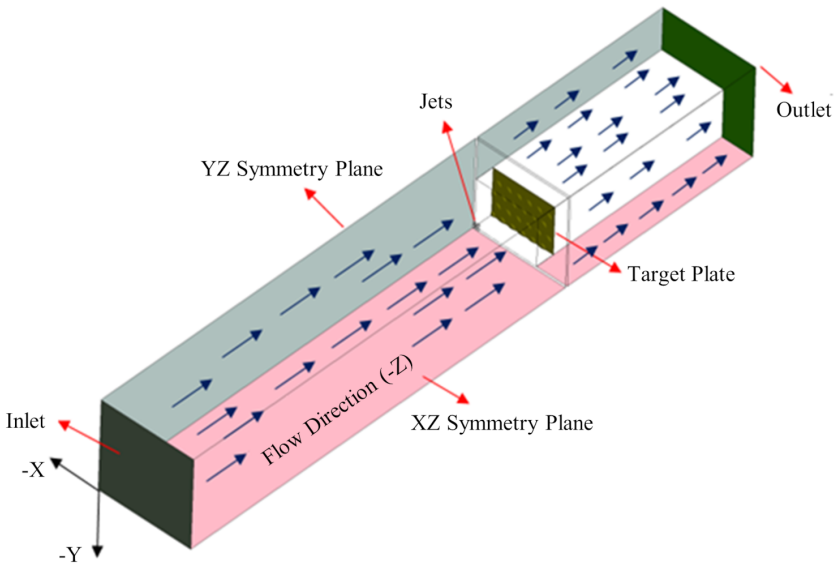

Fig. 6. Schematic diagram of CFD fluid domain

4.1. Meshing

The fluid domain was meshed using the Meshing module of ANSYS. The length of the inlet domain is extended so that flow can be fully developed. At the outlet, an extension in length was also provided to compensate for reverse flows. The whole fluid domain was divided into 3 parts as shown in Fig. 7.

Mesh was generated by considering that all the parameters should lie within the acceptable range. The mesh of the inlet and output domain was achieved with a biased mesh to keep the y^+ value lower than 1. For the inlet and outlet domain, a multi-zone method was used. For the plate domain, the tetrahedral mesh was used along with the inflation layers to capture the boundary layer effects. For the inflation layer, $y^+ < 1$ was used with a first-layer thickness of 0.05 mm and a growth rate of 1.1. Fig. 8 shows the plate domain meshing and inflation layers.

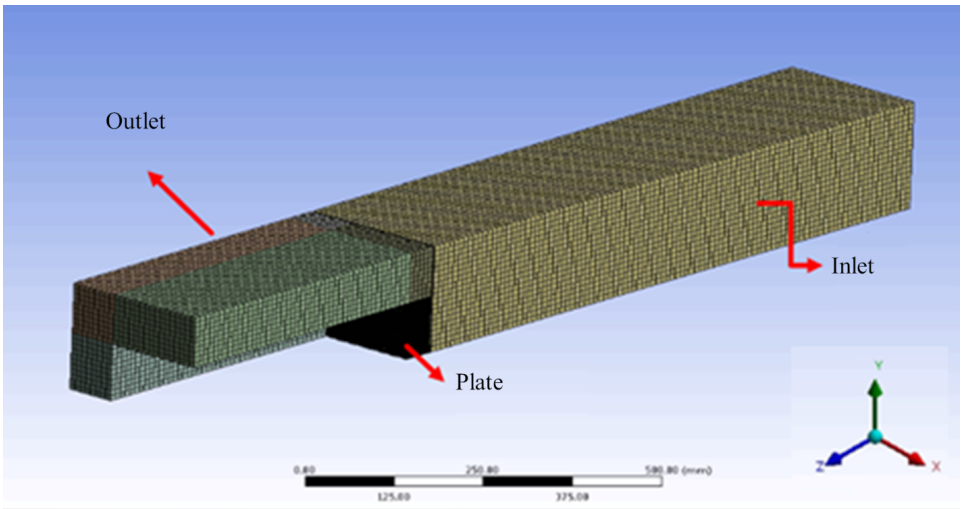

Fig. 7. Schematic diagram of CFD fluid domain

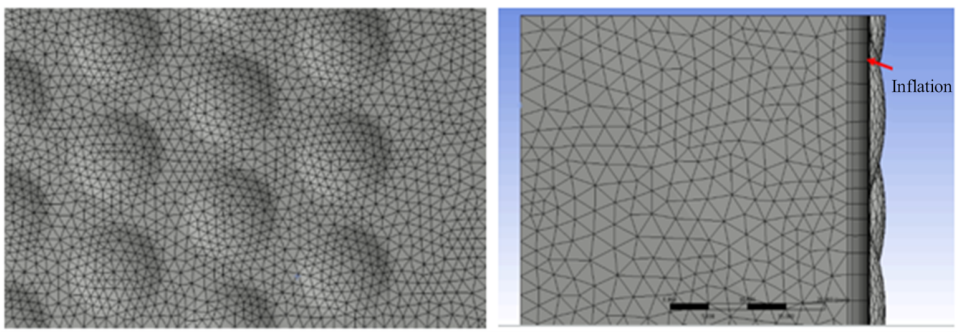

(a) (b)

Fig. 8. (a) Plate domain meshing; (b) Inflation layers

4.2. Grid independence study

A mesh independence study was accomplished so that the results could be made independent of the mesh size. The plate domain, which is near the jet, was finely meshed and the size of the cell in this region was selected to be 1.5 mm after the mesh independence study. The cause for fine meshing was to capture the effects of gradients near the jet plate because of the sharp increase in the velocity of fluid when it crosses the jet section. Mesh sizes were varied to different sizes of 3.5 mm, 3.0 mm, 2 mm, 1.5 mm, and 1.0 mm. The part other than the jet section has coarse mesh with a mesh size of 10 mm. The size of the element for this domain was selected to be 20 mm after mesh independence with a maximum error of 0.5%. Fig. 9 shows the Nusselt number values for different mesh sizes.

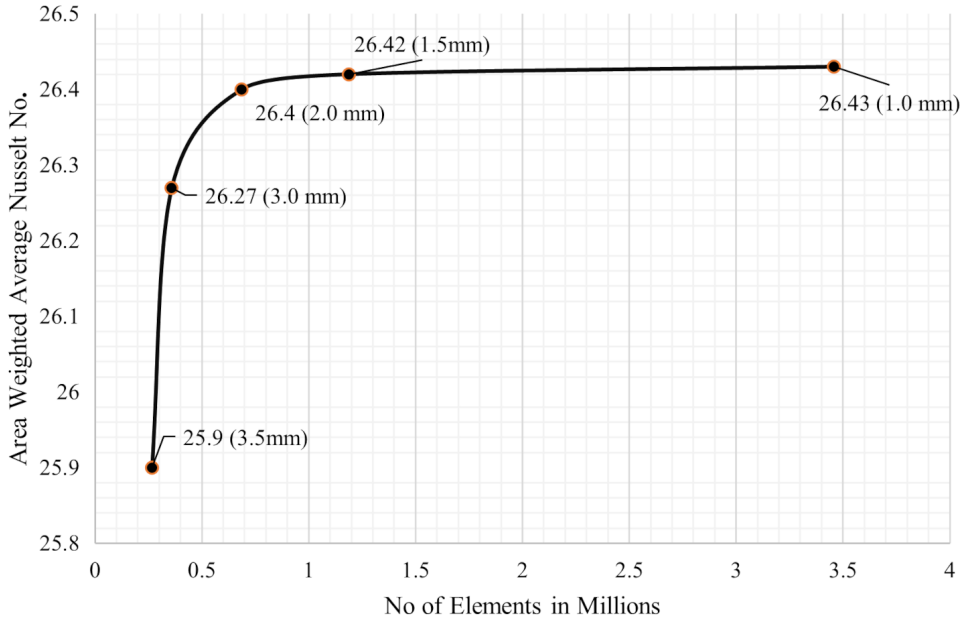

Fig. 9. Mesh independence study

4.3. Selection of turbulence model

Flow phenomenon and geometrical constraints play an important role in choosing the appropriate turbulence model. Flow separation, re-circulations, re-attachment, and swirling flow are the characteristics of dimples or protrusions [31]. Therefore, the validation of numerical results through the experimental study is the primary criterion for selecting a turbulence model. Different turbulence models were tested, but the one that closely matched the experimental results was the standard k-ε with enhanced wall treatment model. This turbulence model was selected for the current study for the closure of RANS because this model provides fairly good results at low and high Reynolds numbers. Fig. 10 illustrates the percentage difference in the experimental and CFD results of the velocity of jet, pressure drop across jet plate and the Nusselt number on target plate for various turbulence models. The experimental results are presented in Table 2. The standard k-ε model shows the lowest overall percentage difference in comparison with other models.

4.4. Boundary and flow conditions

The boundary condition is an integral part of the mathematical model as the whole solution depends upon these conditions. The boundary conditions used for the analysis are listed in Table 1.

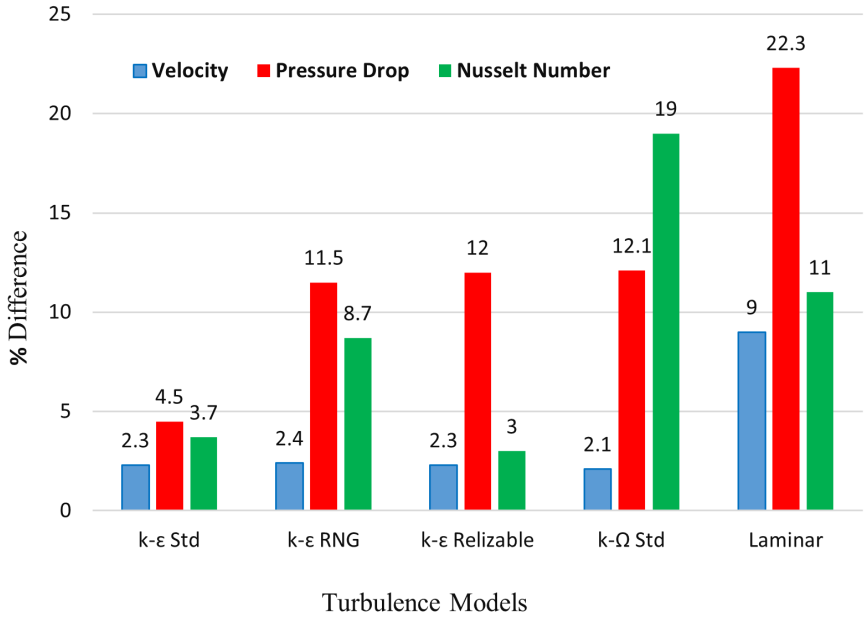

Fig. 10. Percentage difference in experimental and CFD results for various turbulence models

Table 1. Boundary conditions used for the analysis

Parameters	Specifications
Mass flow inlet condition (kg/s)	$(1.3–3.3) \cdot 10^{-3}$
Pressure outlet (Pa)	Gauge zero
Constant heat flux to plate (W/m^2)	330
No-slip and adiabatic	$u = v = \dfrac{\partial T}{\partial y} = 0$
Turbulent intensity	$I = 0.16\mathrm{Re}_d^{-1/8}$
Air temperature at inlet (K)	300

4.5. Solution setup

Continuity, momentum, and energy equations are solved for fully developed, steady-state 3-D turbulent cases. The concerned mathematical equations can be found in the numerical study of Siddiqui et al. [10]. The minimum convergence criterion for the continuity and energy equation has been set to be 10^{-3} and 10^{-7}, respectively. The SIMPLE discretization scheme was used for pressure velocity coupling and the second-order upward scheme was used for momentum, pressure, turbulent kinetic energy, and turbulent dissipation rate.

5. Results and discussion

5.1. Validation

According to the 10, standard k-epsilon with enhanced wall treatment turbulence is selected for CFD analysis of plate configurations. A comparison of experimental results and CFD results for dimple plate is provided in Table 2 where it can be seen that the percentage difference between numerical and experimental cases is within the acceptable range. Additionally, the experimental and the CFD values of the Nusselt number fall within the uncertainty analysis range.

Table 2. Comparison of CFD and experimental results

Sr. No.	Parameters	Results		% Difference
		CFD	Experimental	
1	Velocity of jet (m/s)	8.1	8.3	2.3
2	Pressure drop (Pa)	51.6	54.1	4.5
3	Nusselt number (–)	8.9	9.2	3.7

5.2. Comparative study of artificial roughness

To select the optimized type of turbulators, a CFD study was performed on smooth, dimpled, dimpled-protruded, protruded-dimpled, and protruded configurations for the dimpled plate with an imprint diameter of 20 mm, height/imprint diameter ratio (H/D) of 0.1, and pitch/imprint diameter ratio (P/D) of 0.8 at the Reynolds number of 3000.

5.2.1. Flow and thermal profiles

The variation of static temperature and pressure is shown in Fig. 11, in the spanwise direction. The jets of air, when strike the target plate, lead to a low temperature in the center. When this heated fluid, spreads in the span-wise and stream-wise direction, as a result of impact, it loses its further ability to cool the target plate. The pressure profile follows an opposite trend because the pressure of the jets of air is higher in the center and it abruptly dropped down, due to the spread of the fluid in both x and y directions. Some localized hot spots also appear in the protrusions region, due to flow separation.

Fig. 12 shows the normalized average temperature values for different plate configurations. It can be seen that the protrusion plate shows the maximum improvement in average plate temperature, i.e., the increase in air T_{bulk} is highest for this case. This is due to the fact that the protrusions cause a breakage of the viscous sub-layer and therefore a vigorous mixing takes place. In the cases of dimples, the flow gets trapped and remains in contact with the surface for a longer period of

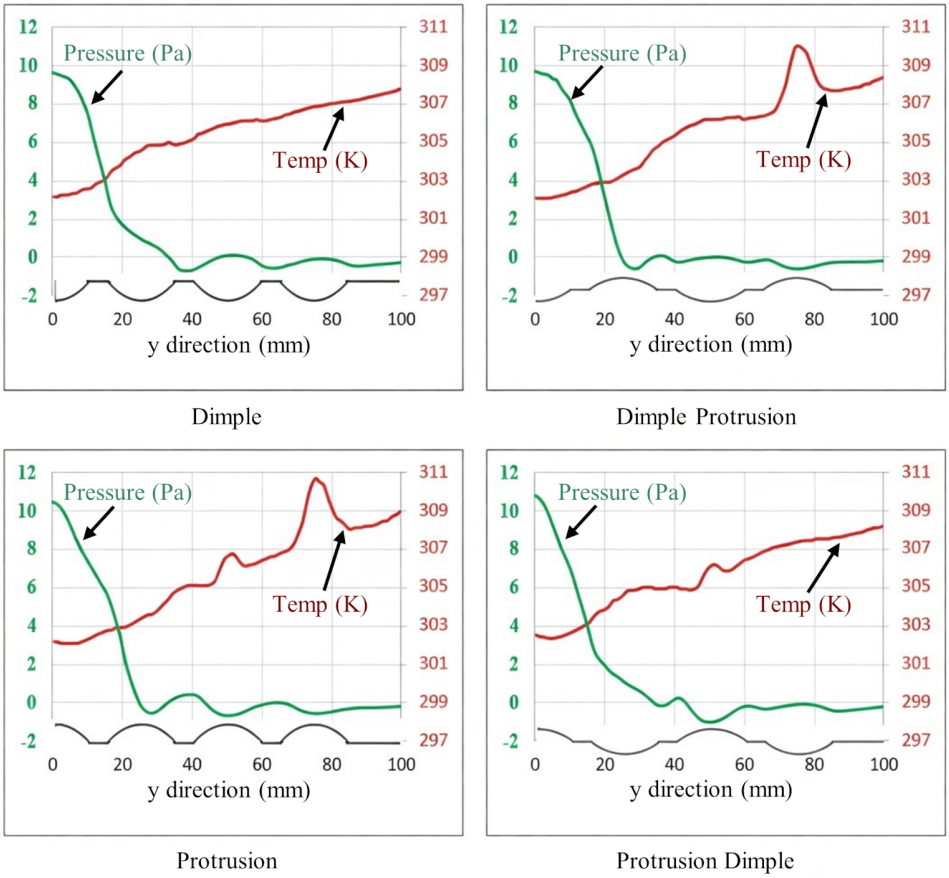

Fig. 11. Pressure and temperature variation in the y direction for different plate configurations

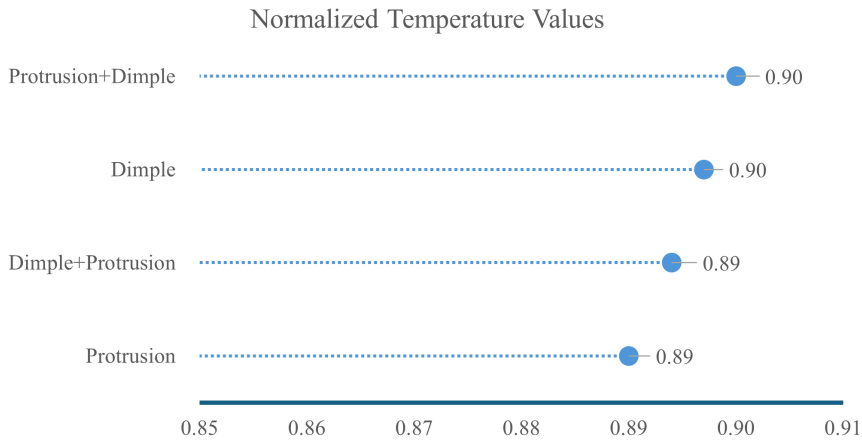

Fig. 12. Comparison of normalized plate temperature for different plate configurations

time, without being replenished by the colder fluid. As a result of this, the overall heat dissipation is affected, as compared to the protrusion case.

Fig. 13 shows the comparison of pressure drop for different plate configurations. The data shows the normalized pressure drop, which is the ratio of the pressure drop in the current configuration to the pressure drop in the case of smooth plate. The pressure drop values for all the plate configurations are almost the same. This is due to the fact that the pressure drop primarily depends on the Reynolds number and not on other plate parameters such as D_i, height, and pitch. For large plate sections, a considerable amount of pressure drop due to height, diameter and pitch, etc., can be achieved, but for smaller plate sizes (307 × 212 mm), the difference is not significant.

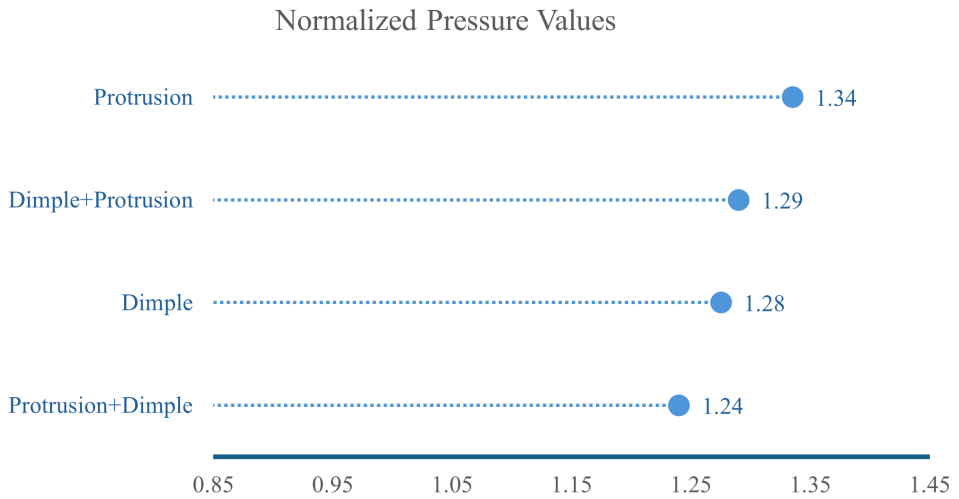

Fig. 13. Comparison of normalized pressure drop for different plate configurations

5.2.2. Velocity contours

The contours of velocity in the vicinity of the target plate are presented in Fig. 14. The maximum velocity is seen in the center, followed by the gradual decline in the magnitudes, due to the spread of fluid in both directions.

5.2.3. Nusselt number

The contours of the Nusselt number are presented in Fig. 15. As a result of the jet strike, the mid-portion of the plate has an overall high rate of heat transfer. After striking the target plate, fluid travels in the X and Y directions and the temperature of fluid increases, leading to a decrease in the Nusselt number values. Fig. 16 shows the comparison of the normalized Nusselt number for different plate configurations. The data shows the average Nusselt number values normalized using

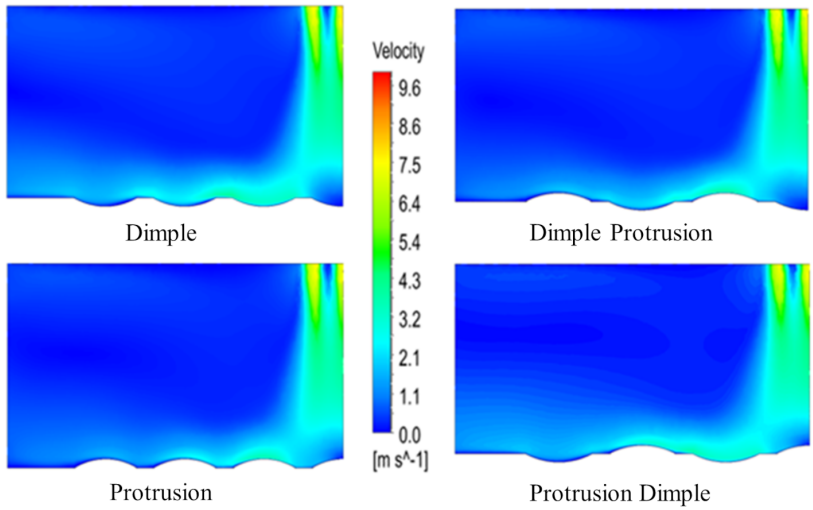

Fig. 14. Velocity contours for different plate configurations

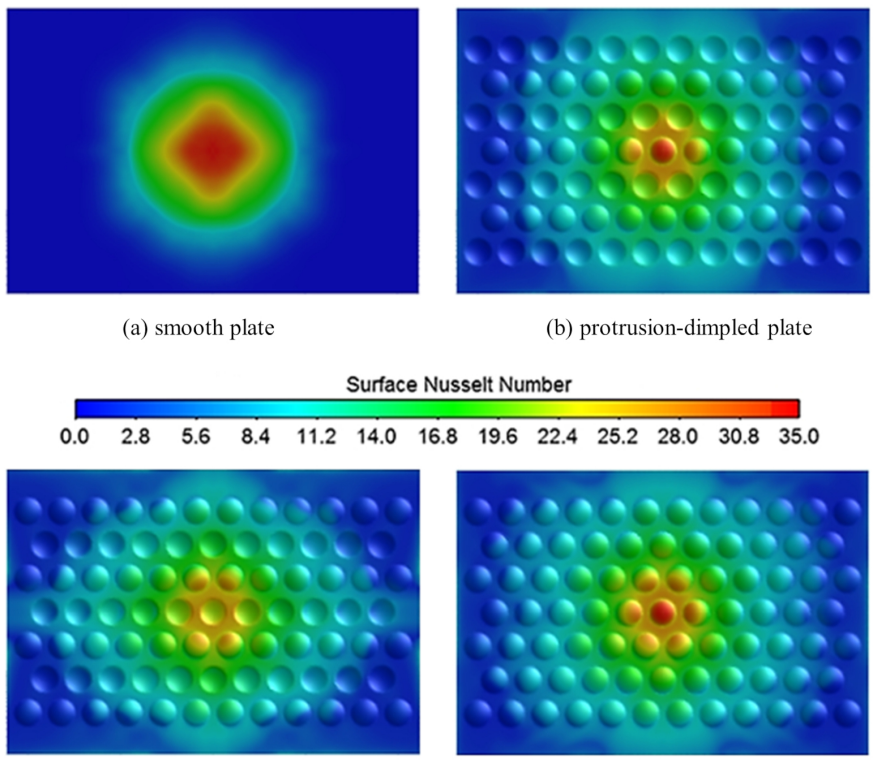

(a) smooth plate (b) protrusion-dimpled plate

(c) dimple protruded plate (d) protruded plate

Fig. 15. (a)–(d)

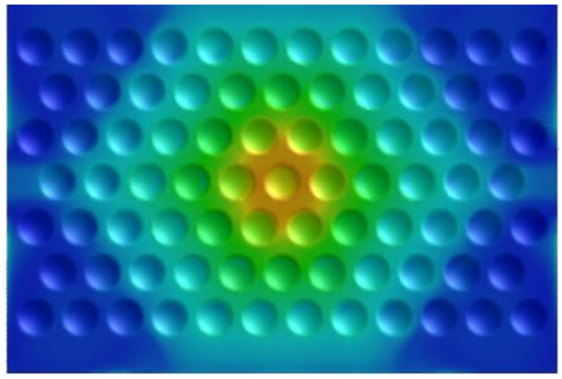

(e) dimpled plate

Fig. 15. The Nusselt number contours for different plate configurations

the smooth plate. The protrusion case exhibits the best results for the normalized Nusselt number as compared to other cases, followed by the protruded-dimpled configuration. A significant rise in the Nusselt number was observed, which was due to the increase in heat transfer area and effects of recirculation effects due to flow turbulence.

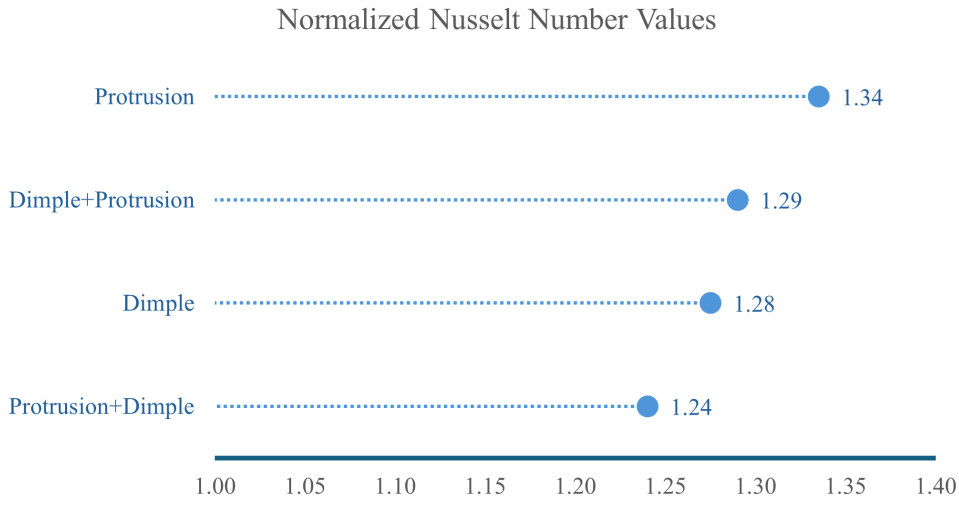

Fig. 16. Contours of the Normalized Nusselt number for different plate configurations

Compared to the dimpled geometry, the protruded one shows a rise in the Nusselt number thanks to continuous replacement of the cooled fluid. In the case of dimpled geometry, the fluid gets trapped, and it leads to the high temperature caused by recirculation of the flow.

5.2.4. Thermal performance factor

The comparison of the Thermal Performance Factor is presented in Fig. 17. As there is no significant difference in the pressure drop among all the cases, so the TPF shows a trend similar to the Nusselt number. An increase of 32% was observed in the protruded configuration, as compared to the smooth plate.

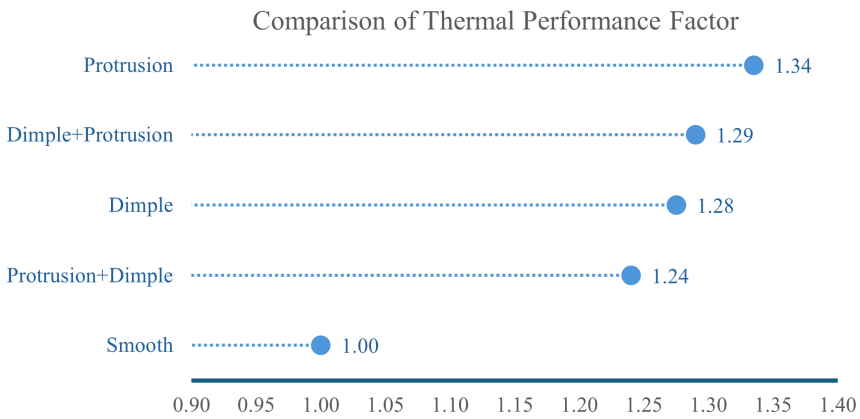

Fig. 17. Comparison of Thermal Performance Factor for different plate configurations

5.3. Inline vs. staggered plate arrangement

After the selection of the protrusion plate as the optimized geometry among the other four plate configurations, simulations using the inline and staggered configurations of the protrusion plate were performed using the validated CFD model. Table 3 shows the better thermal performance of inline arrangement, as compared to staggered arrangement for perpendicular jet impingement arrangement.

Table 3. Inline and staggered configuration comparison

Sr. No.	Parameter	Configuration	
		Inline	Staggered
1	Pressure drop (Pa)	45.5	45.8
2	Avg. Nusselt number	9.7	9.5
3	Thermal performance factor	1.37	1.32

6. Conclusions

Solar energy is considered a clean, cheap, suitable, sustainable, safe, abundant, and economical source. SAH is one of the important utilization of solar energy. SAH has an extensive range of applications with low thermal efficiency. The low

thermal efficiency is mainly due to the inadequate heat transfer between the absorbing medium and air. To improve thermal efficiency, the novel arrangement of a dimple/protrusion absorbing plate with jet impingement is used. Experimental and numerical work have been performed for five different plate configurations with a 3×3 jet array. CFD is used to investigate heat transfer enhancement, the average Nusselt number, pressure drop, and average plate temperature for different configurations. The best configuration was selected based on the thermal performance factor (η). The accomplished work and main conclusions are summarized below:

1. Protruded geometry seems to be the best configuration, followed by dimpled-protruded configuration.
2. An overall improvement of 33.5% is observed in current research work. Hence promising is the augmentation.
3. Inline configuration has slightly better thermal performance, as compared to the staggered arrangement.

The next phase of this research work is based on the study of variation of different geometric and flow parameters, i.e., D_i, H/D_i ratio, P/D_i ratio, and the Reynolds number, using Taguchi Statistical Method.

References

[1] S. Chaudry, P.A. Bahri, and N.R. Moheimani, Pathways of processing of wet microalgae for liquid fuel production: A critical review, *Renewable and Sustainable Energy Reviews*, 52:1240–1250, Dec. 2015. doi: 10.1016/j.rser.2015.08.005.

[2] T.S. Kumar, N.S. Thakur, A. Kumar, and V. Mittal, Use of artificial roughness to enhance heat transfer in solar air heaters – a review, *Journal of Energy in Southern Africa*, 21(1):35–51, Feb. 2010. doi: 10.17159/2413-3051/2010/v21i1a3248.

[3] A. Tayyab, W. Siddique, A. Raheem, T. Salameh, K. Waheed, and K. Qureshi, Effect of various configurations of permeable ribs on thermal performance of solar air heater as source of clean energy, *International Journal of Ambient Energy*, 44(1):31–45, Dec. 2023, doi: 10.1080/01430750.2022.2068064.

[4] W. Siddique et al., Evaluation of thermal performance factor for solar air heaters with artificially roughened channels, *Archive of Mechanical Engineering*, 68(2):195–225, 2021. doi: 10.24425/ame.2021.137048.

[5] G.K. Chhaparwal et al., Numerical and experimental investigation of a solar air heater duct with circular detached ribs to improve its efficiency, *Case Studies in Thermal Engineering*, 60:104780, Aug. 2024. doi: 10.1016/j.csite.2024.104780.

[6] T. Salameh, W. Siddiuue, A. Raheem, and A.H. Al Alami, Evaluation of Thermal Performance Factor of Novel Two-Pass, Ribbed, U-Shaped Channel for Solar Air Heater, in *2020 Advances in Science and Engineering Technology International Conferences* (ASET), 2020, pp. 1–4. doi: 10.1109/ASET48392.2020.9118194.

[7] A. Raheem et al., The effect of corrugation on heat transfer and pressure drop in a solar air heater: a numerical investigation, *Heat Transf. Res.*, 55(9):35–54, 2024. doi: 10.1615/HeatTransRes.2024050336.

[8] A. Raheem et al., Thermal Performance Factor of Impinging Jet-Angled Corrugated Solar Air Heaters, *Energy Technology*, 12(5), May 2024. doi: 10.1002/ente.202301140.

[9] A. Raheem et al., CFD analysis of novel two-pass, sinusoidal corrugated, trapezoidal channel for solar air heater, *International Journal of Ambient Energy*, 45(1):1–18, Dec. 2024. doi: 10.1080/01430750.2024.2326161.

[10] W. Siddique et al., Numerical Investigation of Thermal Performance Factor in Dimpled-Solar Air Heater (SAH), *International Journal of Ambient Energy*, pp. 1–30. doi: 10.1080/01430750.2023.2280754.

[11] A. Raheem et al., Performance evaluation of adding Helical-screw Tape Inserts in Parabolic Solar Trough Collectors as a Source of Cleaner Energy Production, *J. Clean. Prod.*, 297:126628, 2021. doi: 10.1016/j.jclepro.2021.126628.

[12] N. Dharmakkan et al., A case study on analyzing the performance of microplate heat exchanger using nanofluids at different flow rates and temperatures, *Case Studies in Thermal Engineering*, 44:102805, Apr. 2023. doi: 10.1016/j.csite.2023.102805.

[13] A. Raheem et al., To Evaluate the Thermal Performance of Molten Salt Coolants for Parabolic Trough Collectors., *International Journal of Energy for a Clean Environment*, 2024. doi: 10.1615/InterJEnerCleanEnv.2024051859.

[14] R. P. Saini and J. Verma, Heat transfer and friction factor correlations for a duct having dimple-shape artificial roughness for solar air heaters, *Energy*, 33(8):1277–1287, Aug. 2008. doi: 10.1016/j.energy.2008.02.017.

[15] V. Goel, R. Kumar, S. Bhattacharyya, V.V. Tyagi, and A. M. Abusorrah, A comprehensive parametric investigation of hemispherical cavities on thermal performance and flow-dynamics in the triangular-duct solar-assisted air-heater, *Renew. Energy*, 173:896–912, Aug. 2021. doi: 10.1016/j.renene.2021.04.006.

[16] A.K. Hassan, M. Muzaffarul Hasan, and M. Emran Khan, Parametric investigation and correlation development for heat transfer and friction factor in multiple arc dimple roughened solar air duct, *Renew. Energy*, 174:403–425, Aug. 2021. doi: 10.1016/j.renene.2021.03.044.

[17] A. Perwez and R. Kumar, Thermal performance investigation of the flat and spherical dimple absorber plate solar air heaters, *Solar Energy*, 193:309–323, Nov. 2019. doi: 10.1016/j.solener.2019.09.066.

[18] L.M. Wright and J.-C. Han, Heat Transfer Enhancement for Turbine Blade Internal Cooling, in Volume 3: Gas Turbine Heat Transfer; Transport Phenomena in Materials Processing and Manufacturing, *American Society of Mechanical Engineers*, Jul. 2013. doi: 10.1115/HT2013-17813.

[19] M.M. Matheswaran et al., A case study on thermo-hydraulic performance of jet plate solar air heater using response surface methodology, *Case Studies in Thermal Engineering*, 34, p. 101983, Jun. 2022. doi: 10.1016/j.csite.2022.101983.

[20] A.J. Robinson and E. Schnitzler, An experimental investigation of free and submerged miniature liquid jet array impingement heat transfer, *Exp. Therm. Fluid Sci.*, 32(1):1–13, Oct. 2007. doi: 10.1016/j.expthermflusci.2006.12.006.

[21] R. Nadda, A. Kumar, and R. Maithani, Developing heat transfer and friction loss in an impingement jets solar air heater with multiple arc protrusion obstacles, *Solar Energy*, 158:117–131, Dec. 2017. doi: 10.1016/j.solener.2017.09.042.

[22] T. Rajaseenivasan, S. Ravi Prasanth, M. Salamon Antony, and K. Srithar, Experimental investigation on the performance of an impinging jet solar air heater, *Alexandria Engineering Journal*, 56(1):63–69, Mar. 2017. doi: 10.1016/j.aej.2016.09.004.

[23] R. Chauhan and N.S. Thakur, Heat transfer and friction factor correlations for impinging jet solar air heater, *Exp. Therm. Fluid Sci.*, 44:760–767, Jan. 2013, doi: 10.1016/j.expthermflusci.2012.09.019.

[24] A.M. Aboghrara, B.T.H.T. Baharudin, M.A. Alghoul, N.M. Adam, A.A. Hairuddin, and H.A. Hasan, Performance analysis of solar air heater with jet impingement on corrugated absorber plate, *Case Studies in Thermal Engineering*, 10:111–120, Sep. 2017. doi: 10.1016/j.csite.2017.04.002.

[25] R. Maithani, S. Sharma, and A. Kumar, Thermo-hydraulic and exergy analysis of inclined impinging jets on absorber plate of solar air heater, *Renew. Energy*, 179:84–95, Dec. 2021. doi: 10.1016/j.renene.2021.07.013.

[26] S. Singh, S.K. Chaurasiya, B.S. Negi, S. Chander, M. Nemś, and S. Negi, Utilizing circular jet impingement to enhance thermal performance of solar air heater, *Renew. Energy*, 154:1327–1345, Jul. 2020. doi: 10.1016/j.renene.2020.03.095.

[27] M.M. Matheswaran, T.V. Arjunan, and D. Somasundaram, Analytical investigation of solar air heater with jet impingement using energy and exergy analysis, *Solar Energy*, 161:25–37, Feb. 2018. doi: 10.1016/j.solener.2017.12.036.

[28] S. Yadav and R.P. Saini, Numerical investigation on the performance of a solar air heater using jet impingement with absorber plate, *Solar Energy*, 208:236–248, Sep. 2020. doi: 10.1016/j.solener.2020.07.088.

[29] T. Alam and M.-H. Kim, Heat transfer enhancement in solar air heater duct with conical protrusion roughness ribs, *Appl. Therm. Eng.*, 126:458–469, Nov. 2017. doi: 10.1016/j.applthermaleng.2017.07.181.

[30] A. Raheem et al., Heat Transfer Enhancement of Impinging Jet-Corrugated Solar Air Heaters, *J. Sol. Energy Eng.*, 2024. doi: 10.1115/1.4064503.

[31] W. Siddique et al., Numerical investigation of thermal performance factor in dimpled-Solar Air Heater (SAH)', *International Journal of Ambient Energy*, 45(1), Dec. 2024. doi: 10.1080/01430750.2023.2280754.